PTEP

Prog. Theor. Exp. Phys. **2018**, 021D01 (8 pages)
DOI: 10.1093/ptep/pty011

Letter

Exclusive quasi-free proton knockout from oxygen isotopes at intermediate energies

Shoichiro Kawase[1,14,*], Tomohiro Uesaka[2], Tsz Leung Tang[1], Didier Beaumel[3], Masanori Dozono[1], Taku Fukunaga[4], Toshihiko Fujii[1], Naoki Fukuda[2], Alfredo Galindo-Uribarri[5], Sanghoon Hwang[6,15], Naoto Inabe[2], Takahiro Kawabata[7], Tomomi Kawahara[8], Wooyoung Kim[6], Keiichi Kisamori[1], Motoki Kobayashi[1], Toshiyuki Kubo[2], Yuki Kubota[1], Kensuke Kusaka[2], Cheongsoo Lee[1], Yukie Maeda[9], Hiroaki Matsubara[1], Shin'ichiro Michimasa[1], Hiroyuki Miya[1], Tetsuo Noro[4], Yuki Nozawa[7,16], Alexandre Obertelli[10,17], Kazuyuki Ogata[11], Shinsuke Ota[1], Elizabeth Padilla-Rodal[12], Satoshi Sakaguchi[2,4], Hideyuki Sakai[2], Masaki Sasano[2], Susumu Shimoura[1], Samvel Stepanyan[6], Hiroshi Suzuki[2], Tomokazu Suzuki[11], Motonobu Takaki[1], Hiroyuki Takeda[2], Atsushi Tamii[11], Hiroshi Tokieda[1], Tomotsugu Wakasa[4], Takashi Wakui[13], Kentaro Yako[1], Jumpei Yasuda[4], Yoshiyuki Yanagisawa[2], Rin Yokoyama[1], Kazuki Yoshida[11], Koichi Yoshida[2], and Juzo Zenihiro[2]

[1]*Center for Nuclear Study, University of Tokyo, 2-1 Hirosawa, Wako, Saitama 351-0198, Japan*
[2]*RIKEN Nishina Center for Accelerator-based Science, Wako, Saitama 351-0198, Japan*
[3]*Institut de Physique Nucléaire d'Orsay, 91406 Orsay, France*
[4]*Department of Physics, Kyushu University, Fukuoka, Fukuoka 819-0395, Japan*
[5]*Oak Ridge National Laboratory, TN 37831, USA*
[6]*Department of Physics, Kyungpook National University, Daegu 41566, Republic of Korea*
[7]*Department of Physics, Kyoto University, Kyoto, Kyoto 606-8502, Japan*
[8]*Department of Physics, Toho University, Funabashi, Chiba 274-8510, Japan*
[9]*Department of Applied Physics, University of Miyazaki, Miyazaki, Miyazaki 889-2192, Japan*
[10]*IRFU, CEA, Université Paris-Saclay, 91191 Gif-sur-Yvette, France*
[11]*Research Center for Nuclear Physics, Osaka University, Ibaraki, Osaka 567-0047, Japan*
[12]*Instituto de Ciencias Nucleares, Universidad Nacional Autónoma de México, 04510 México D.F., Mexico*
[13]*Cyclotron and Radioisotope Center, Tohoku University, Sendai, Miyagi 980-8578, Japan*
[14]*Present address: Department of Advanced Energy Engineering Science, Kyushu University, Kasuga, Fukuoka 816-8580, Japan*
[15]*Present address: Korea Research Institute of Standards and Science (KRISS), Daejeon 34113, Republic of Korea*
[16]*Present address: RCNP, Osaka University, Ibaraki, Osaka 567-0047, Japan*
[17]*Present address: Institut für Kernphysik, Technische Universität Darmstadt, 64289 Darmstadt, Germany*
*E-mail: kawase@aees.kyushu-u.ac.jp

Received October 26, 2017; Revised January 3, 2018; Accepted January 19, 2018; Published February 28, 2018

The dependence of the single-particle strength on the difference between proton and neutron separation energies is studied for oxygen isotopes in a wide range of isospins. The cross sections of the quasi-free $(p, 2p)$ reaction on ^{14,16,18,22,24}O were measured at intermediate energies. The measured cross sections are compared to predictions based on the distorted wave impulse approximation and shell-model *psd* valence-space spectroscopic factors. The reduction factors, which are the ratio of the experimental cross sections to the theoretical predictions, show no apparent dependence on the proton–neutron separation energy difference. The result is compatible with the result of the $(e, e'p)$ reaction on stable targets and with the predictions of recent *ab initio* calculations.

Subject Index D13, D27

1. *Introduction* The occupation probability of single-particle orbits is one of the important properties characterizing the nuclear structure. In the independent-particle picture, it is by definition unity for orbits below the Fermi surface and zero for those above. The existence of nucleon–nucleon (NN) correlations, such as the short-range correlation, the pairing correlation, and the tensor correlation, reduces the single-particle strength in nuclei [1]. Experimentally, this reduction can be investigated by using single-nucleon addition and removal reactions. In the experiments, the spectroscopic factor (SF), which is defined as the ratio of the measured cross section to that calculated with a unit occupation number, is widely used as a measure of the occupation probability. It is well known that the SF is subject to typically $\sim$30% reduction from the shell-model calculation due to the NN correlations, which is not fully included in the theoretical model [2,3]. For the stable nuclei, the reduction factor is known to be an almost constant value of $\sim$0.7 and the quenching mechanism is considered to be universal over the nuclear chart.

Recently, strong dependence of the reduction factors on nucleon separation energies has been inferred from the interpretation of one-nucleon-removal reactions at energies of about 70–130 MeV/nucleon with nuclear targets [4,5]. The former study suggested enhanced correlations, which scatter nucleons at higher energy, for deeply bound nucleons. This study triggered measurements of single-particle strengths in unstable nuclei with multiple reaction probes. Good examples of that are studies with transfer reactions, where the strong dependence was not observed [6,7].

In this article, the reduction factors in the single-proton-removal reaction from oxygen isotopes are investigated for a wide isotopic chain of $A = 14$–24 using the quasi-free $(p, 2p)$ reaction. The quasi-free $(p, 2p)$ reaction at intermediate energies is one of the most transparent hadronic reactions because (i) only one nucleon is involved as a target and (ii) the NN scattering cross section takes its minimum at 200–400 MeV. This allows one to probe the relatively large volume of a nucleus compared to low-energy transfer reactions and nucleon-removal reactions with nuclear targets. Thus, experimental studies with $(p, 2p)$ reactions can shed new light on the problem. In addition, the $(p, 2p)$ reaction can accompany large momentum transfer and does not strongly depend on the kinematical matching condition, as is the case in transfer reactions. This feature is preferable in systematic studies, because beams with different mass change the kinematical conditions.

2. *Experiment* This experiment was performed at the RI Beam Factory (RIBF) [8] operated by the RIKEN Nishina Center and CNS, University of Tokyo by using ^{14,22,24}O beams at 250 MeV/nucleon. The ^{16,18}O data at 200 MeV/nucleon were obtained at the Research Center for Nuclear Physics (RCNP), Osaka University. In the following, details of the RIBF experiment will be described, while those of the RCNP experiment will be reported elsewhere. The unstable secondary beams were produced through projectile fragmentation of a 345 MeV/nucleon ^{48}Ca primary beam on a ^{9}Be production target with thicknesses of 5 mm (^{14}O), 20 mm (^{22}O), and 30 mm (^{24}O). The beam was transported and separated in the BigRIPS in-flight fragment separator [9]. Particle identification (PID) of beam particles was carried out event-by-event by using their time of flight (TOF) and energy loss (ΔE) in plastic scintillators after $B\rho$ separation. Then the secondary beam bombarded a hydrogen target made of naphthalene [10]. The number density of hydrogen atoms in the target was 4.45×10^{21} cm^{-2}. The relative uncertainty of the target thickness was estimated to be $\pm$3%; this is due to the uncertainty of the weight and the cross section measurement. The target impurity was negligible in this experiment.

To obtain the triple differential cross section $d^3\sigma/(dE_1 d\Omega_1 d\Omega_2)$ for the $(p, 2p)$ reaction, the momentum vectors of the beam particle and the two outgoing protons were determined. The energy

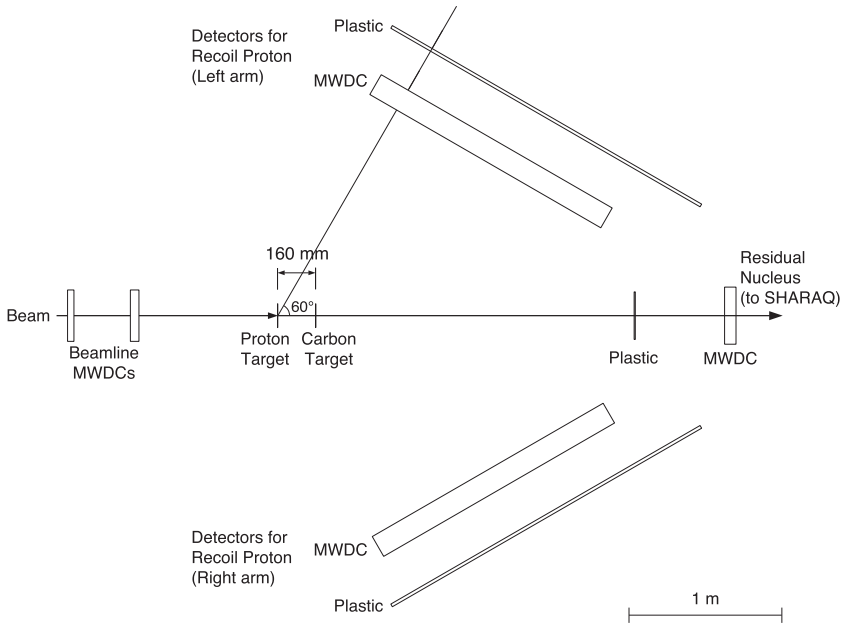

Fig. 1. Schematics of the experimental setup in the target area.

of the beam is calculated from the $B\rho$ value of the central trajectory, which was measured by using NMR at the BigRIPS dipole magnet and from the beam trajectory at the momentum-dispersive focal plane. The momenta of the two scattered protons were determined by using the multiwire drift chambers [11] and plastic scintillators located both (left and right) sides of the beamline. The proton detection efficiency in the acceptance was 91% for each detector arm. Figure 1 shows the schematics of the setup in the target area. Detectors are shown as rectangles with the size representing their effective areas.

Since the naphthalene target used as a proton target in the present experiment includes carbon, cross sections for the carbon were simultaneously measured by using a pure carbon target with a thickness of 0.6 mm, which was located 160 mm downstream of the reaction target. The reaction vertex was identified from the trajectories of the beam and the scattered protons. The position resolution of the vertex point along the beam direction was $\sim$ 10 mm.

The $(p, 2p)$ events of interest were selected by requiring the following conditions: (i) the beam particle is an oxygen isotope of interest, (ii) both of the scattered particles are protons, and (iii) the residual particle is a nitrogen or a carbon isotope. The last condition is necessary to improve the signal-to-noise (S/N) ratio for low-lying states, which are focused on in this study, by eliminating the yield of the various reactions emitting two protons, such as spallation reactions. The residual nucleus was momentum analyzed and identified by the first half (QQD; which consists of two quadrupole magnets and one dipole magnet) of the SHARAQ spectrometer [12]. Figures 2a and 2b show the 2D plots that were used for PID.

The proton separation energy (S_p) of the reaction can be defined as the difference between the total masses before and after the reaction:

$$S_p = (2m_p + m_R) - (m_p + m_T) \tag{1}$$

$$= (1-\gamma)\, m_p - \gamma\,(T_1 + T_2) + \beta\gamma\left(p_{1\parallel} + p_{2\parallel}\right) - \frac{k^2}{2m_R}, \tag{2}$$

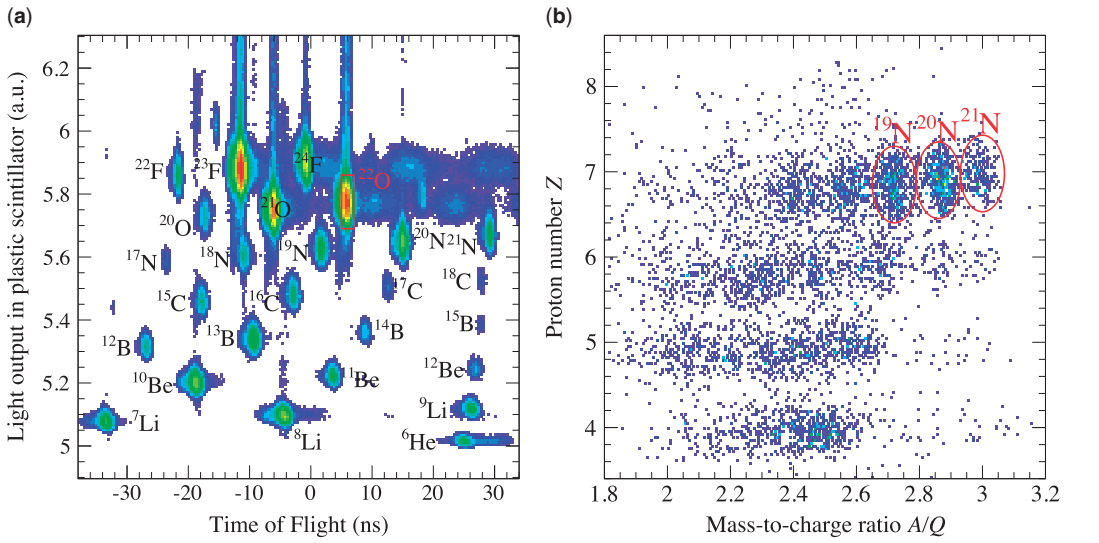

PID plot for the secondary beam.

PID plot for the residual particles under the condition that two protons are detected in both detector arms.

Fig. 2. Particle identification (PID) plots in ^{22}O runs.

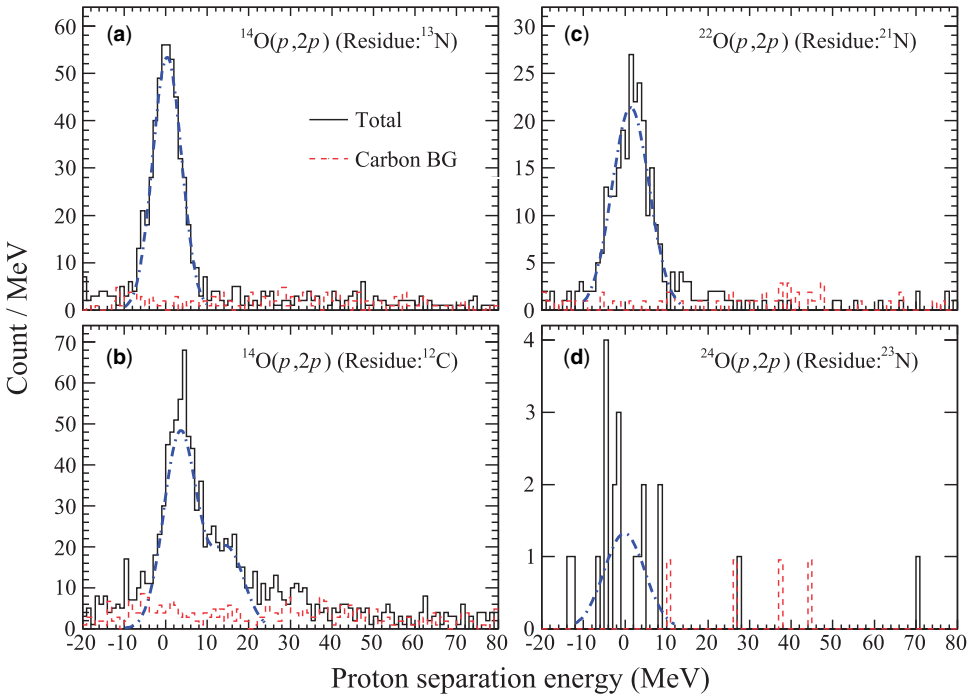

Fig. 3. Proton separation energy spectra for (a) ^{14}O$(p, 2p)$ with residues of ^{13}N, (b) ^{14}O$(p, 2p)$ with residues of ^{12}C, (c) ^{22}O$(p, 2p)$ with residues of ^{21}N, and (d) ^{24}O$(p, 2p)$ with residues of ^{23}N. The red broken lines indicate the background yields from the carbon component in the reaction target. The blue dash-dotted lines shows the fitting result by assuming a Gaussian shape for each state.

where β and γ are the Lorentz factors of the beam particle, T_i and $p_{i\parallel}$ $(i = 1, 2)$ are the kinetic energy and the parallel momentum of the scattered proton, k is the missing momentum, and m_p, m_R, m_T are the masses of proton, residual nuclei, and target nuclei, respectively. As m_R depends on S_p, the calculations were carried out in an iterative way. Figure 3 shows the proton separation energy spectra. Table 1 shows the cross sections ($\sigma_{\rm exp}$) that are obtained by fitting the excitation energy

Table 1. Experimental and theoretical cross sections for the $(p, 2p)$ reaction at 250 MeV/nucleon, SFs, and reduction factors (R_s) for each final state of nitrogen with an excitation energy of $E_x(^{A-1}\mathrm{N})$. The cross sections were integrated in the experimental acceptance. Statistical errors are indicated in parentheses.

Beam	Residue	$E_x(^{A-1}\mathrm{N})$ (MeV)	J^π	σ_{exp} (μb)	$\sigma^{\mathrm{sp}}_{\mathrm{DP}}$ (μb)	$\sigma^{\mathrm{sp}}_{\mathrm{MS}}$ (μb)	$\mathrm{SF}_{\mathrm{SM}}$	$R_{s\mathrm{DP}}$	$R_{s\mathrm{MS}}$
^{14}O	^{13}N	0.0	$p_{1/2}$	385(15)	315	348	1.56	0.78(3)	0.71(3)
		3.5	$p_{3/2}$	398(20)	330	359	1.95		
	^{12}C	9.5	$p_{3/2}$	11(18)	269	299	0.57	0.54(2)	0.50(2)
		15	$p_{3/2}$	158(15)	230	261	1.06		
^{22}O	^{21}N	0.0	$p_{1/2}$	120(8)	107	131	1.84	0.52(3)	0.43(3)
		1.16	$p_{3/2}$		125	144	0.27		
^{24}O	^{23}N	0.0	$p_{1/2}$	114(29)	90	113	1.92	0.66(17)	0.53(13)

spectra assuming a Gaussian shape for each state. The fitting results are shown in Fig. 3 as blue dash-dotted lines. The cross sections are integrated under the condition that both protons have kinetic energy higher than 30 MeV, and over the angular range covering $20^\circ < \theta < 65^\circ$ and $|\phi| < 15^\circ$ (2.52×10^{-1} sr) for each proton-detector arm. Events from both naphthalene and the carbon target are accepted in this angular range.

The cross section decreases as the neutron number increases. This tendency can be reproduced by the theoretical calculations that are described in the following section. It is remarkable that the spectrum in Fig. 3b shows a bump structure at around 15 MeV. This can be attributed to the isobaric analogue state (IAS) of ^{13}O. The large spectroscopic amplitude of the IAS inferred from our data is consistent with the data from the $^{14}\mathrm{C}(d, t)^{13}\mathrm{C}$ reaction measurement [13].

In the present measurement, the ground state (g.s.) and the first excited state of ^{21}N cannot be separated due to insufficient energy resolution. The contribution of each state is estimated from the shell-model calculation in the next section.

3. *Theoretical analysis and discussion*

In order to obtain the reduction factors from the experimental result, the measured cross sections were compared to predictions by the distorted wave impulse approximation (DWIA) [14–16], with shell-model spectroscopic factors. DWIA calculations were made by using THREEDEE [17]. We used single-particle wave functions calculated with a Woods–Saxon (WS) potential with a radius of $r_0 A^{1/3}$ ($r_0 = 1.27$ fm) and diffuseness $a_0 = a_{\mathrm{LS}} = 0.67$ fm. The depth of the WS potential was set to reproduce the experimental separation energy.

In the present study, two optical potentials, the energy-dependent atomic-mass-number-dependent Dirac phenomenology potential (DP) [18] and the microscopic optical model (MS) [19], were used. In the DWIA calculations, attenuation of the distorted waves by the imaginary part of the optical potential can be a major factor in the prediction of absolute values of cross sections. In this respect, the MS model has two noteworthy advantages. In the MS model, optical potentials are calculated by folding the Melbourne g-matrix [20] with proton and deuteron density distributions, which are calculated with the same WS potential as for the single-particle wave functions. This model naturally assures the consistency of the potential parameters for calculations of single-particle wave functions and distorted waves. The other advantage is that this model has explicit isovector dependence through the nuclear density and the Melbourne g-matrix; see Ref. [19] for details. These two features of the MS model, which are missing in the DP model, are quite essential in avoiding the spurious isospin dependence in cross sections. It is found, however, that in the reaction systems discussed in this

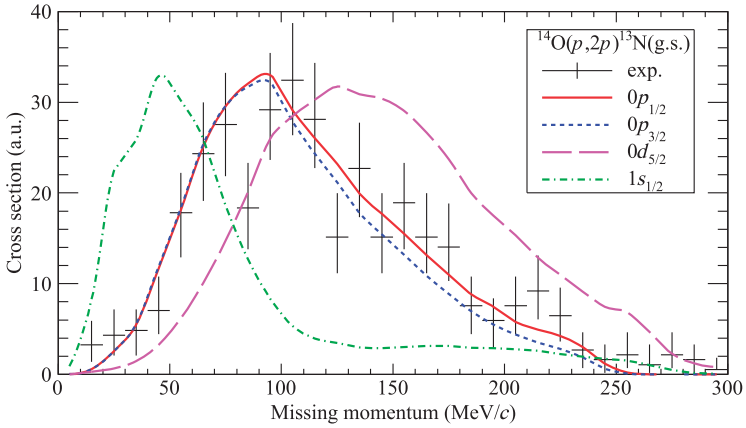

Fig. 4. Missing momentum distribution for the ^{14}O$(p, 2p)^{13}$N(g.s.) reaction.

study, the isovector part of the optical potential is at most about 10% of the isoscalar part. This will be the main reason for the small difference in the reduction factors obtained with the DP and MS potentials, as shown below. Nevertheless, it should be noted that the MS model is considered to be more appropriate when it is applied to unstable isotopes with large differences in proton and neutron numbers.

For the *NN* interaction, we used the density-independent *NN* interaction, which is equivalent to the *NN* phase shifts [21]. The cross sections are obtained by integrating the calculated differential cross sections over the experimental acceptance. The resulting cross sections for a unit spectroscopic factor ($\sigma^{\rm sp}$) are shown in Table 1.

In $(p, 2p)$ reaction measurement, the information on the orbital angular momentum of the struck proton can be obtained by comparing the missing momentum distribution, which reflects the momentum distribution of the struck proton in the nucleus, to the theoretical prediction. For example, Fig. 4 shows the missing momentum distributions for ^{14}O$(p, 2p)^{13}$N(g.s.) in the experimental acceptance, obtained from the measurement and the calculation using the MS potential. The missing momentum distributions for all the reaction channels shown in Table 1 are consistent with the ones obtained from the calculation with the assumption that the struck protons were in $0p$ orbits in oxygen isotopes.

The SFs are estimated from the shell-model calculations with OXBASH [22]. We used the SFO (Suzuki–Fujimoto–Otsuka) interaction [23] as the effective *NN* interaction in the $p+sd$ model space. The obtained SFs for $p_{1/2}$ orbits range from 1.5–2, as shown in Table 1.

Theoretical cross sections obtained by multiplying $\sigma_{\rm sp}$ by SFs are shown in Fig. 5 along with the experimental cross sections ($\sigma_{\rm exp}$). In this figure, the black crosses, the up-pointing red triangles, and the down-pointing blue triangles indicate $\sigma_{\rm exp}$, theoretical cross sections with DP ($\sigma_{\rm DP+SM}$), and those with MS ($\sigma_{\rm MS+SM}$), respectively. As expected, the theoretical cross section is larger than $\sigma_{\rm exp}$ for every reaction channel. MS gives systematically larger cross sections than DP but the difference is $\sim$ 15% at most and thus does not affect the following discussion.

Figure 6 shows the reduction factor defined as $R_s \equiv \sigma_{\rm exp}/\sigma_{\rm theory}$ as a function of the separation energy difference $\Delta S \equiv S_p - S_n$ for proton knockout reactions. The $\sigma_{\rm exp}$, $\sigma_{\rm MS+SM}$, and $\sigma_{\rm DP+SM}$ for ^{16,18}O are obtained in the same procedure. The R_s for ^{16}O is consistent with that obtained in the $(e, e'p)$ measurement [24]. This consistency supports the reliability of the R_s resulting from the $(p, 2p)$ measurements. A similar conclusion is drawn in Ref. [3] for several nuclei, as shown in Figs. 23 and 24 of that reference. The R_s for ^{14}O is comparable to that obtained in the proton-removal

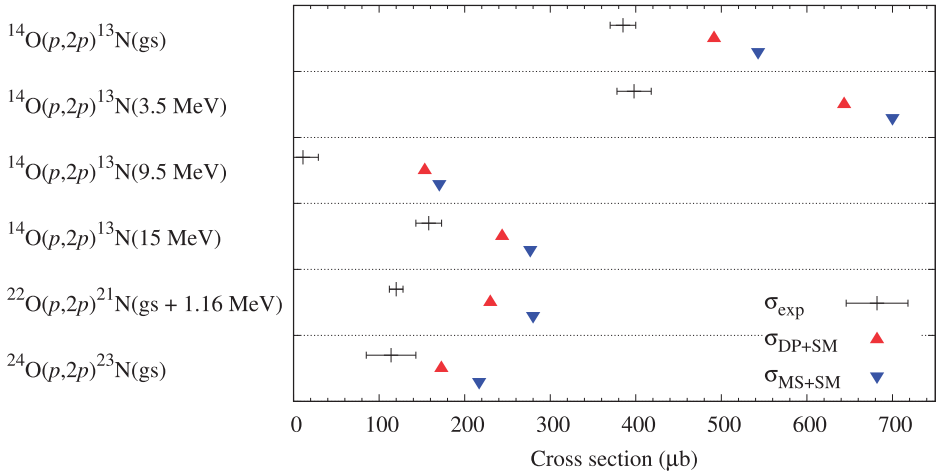

Fig. 5. Measured cross sections (σ_{exp}) and corresponding cross sections calculated by using THREEDEE and OXBASH with the Dirac phenomenology optical potentials (σ_{DP+SM}) and the microscopic optical potentials (σ_{MS+SM}) for each reaction channel.

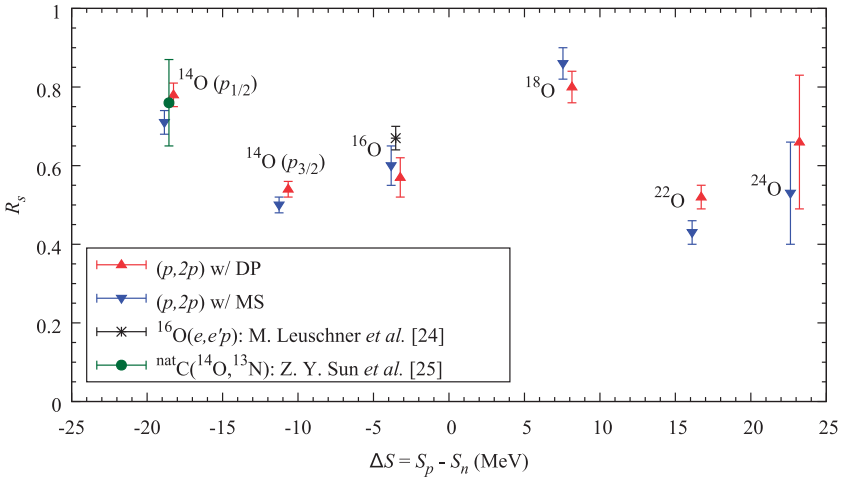

Fig. 6. Reduction factors R_s as a function of separation energy differences ΔS. Up- and down-pointing triangles indicate R_s deduced using DP and MS optical potentials. Results of the $(e, e'p)$ reaction [24] and the proton-removal ^{nat}C(^{14}O,^{13}N) reaction [25] are shown for comparison.

^{nat}C(^{14}O, ^{13}N) reaction at 305 MeV/nucleon [25]. Apparently, no strong ΔS dependence is found in the present result. This contradicts the case of proton knockout reactions with nuclear targets [4,5], and is consistent with those of transfer reaction measurements, such as Refs. [6] and [7]. The present result confirms the predictions of recent *ab initio* calculations [26,27] where the ΔS dependence of R_s is weak. The experimentally observed constancy of the reduction factor indicates that the nuclear correlation effects depend on proton–neutron asymmetry only weakly.

4. *Conclusions* The $(p, 2p)$ reactions on ^{14,16,18,22,24}O at intermediate energies were studied to investigate the reduction factor as a function of the proton-to-neutron separation energy difference in a wide range of isospins. The cross sections for ^{14,22,24}O were measured with 250 MeV/nucleon radioactive nuclear beams at RIBF and those for ^{16,18}O were obtained with the 200 MeV proton beam at RCNP. Experimental cross sections were compared to predictions based on DWIA calculations and

shell-model spectroscopic factors. The reduction factor does not exhibit any apparent dependence on the difference between the proton–neutron separation energies, which is compatible with the result of the $(e, e'p)$ reaction on stable targets and with the predictions of recent *ab initio* calculations.

Acknowledgements

We are grateful to the accelerator staff of the RIKEN Nishina Center for providing a high-intensity radioactive beam at RIBF. The authors also thank the RCNP staff for a high-quality proton beam. One of the authors (S.K.) acknowledges the financial support by a Grant-in-Aid for Japan Society for the Promotion of Science (JSPS) Research Fellow (No. 23-6202).

References

[1] V. R. Pandharipande, I. Sick, and P. K. A. deWitt Huberts, Rev. Mod. Phys. **69**, 981 (1997).
[2] L. Lapikás, Nucl. Phys. A **553**, 297 (1993).
[3] T. Wakasa, K. Ogata, and T. Noro, Prog. Part. Nucl. Phys. **96**, 32 (2017).
[4] A. Gade et al., Phys. Rev. C **77**, 044306 (2008).
[5] J. A. Tostevin and A. Gade, Phys. Rev. C **90**, 057602 (2014).
[6] J. Lee et al., Phys. Rev. Lett. **104**, 112701 (2010).
[7] F. Flavigny et al., Phys. Rev. Lett. **110**, 122503 (2013).
[8] Y. Yano, Nucl. Instrum. Meth. B **261**, 1009 (2007).
[9] T. Kubo, Nucl. Instrum. Meth. B **204**, 97 (2003).
[10] T. Wakui, M. Hatano, H. Sakai, T. Uesaka, and A. Tamii, Nucl. Instrum. Meth. A **550**, 521 (2005).
[11] H. Okamura et al., Nucl. Instrum. Meth. A **406**, 78 (1998).
[12] T. Uesaka, S. Shimoura, and H. Sakai [SHARAQ Collaboration], Prog. Theor. Exp. Phys. **2012**, 03C007 (2012).
[13] M. Yasue et al., Nucl. Phys. A **509**, 141 (1990).
[14] D. F. Jackson and T. Berggren, Nucl. Phys. **62**, 353 (1965).
[15] K. L. Lim and I. E. McCarthy, Phys. Rev. **133**, B1006 (1964).
[16] B. K. Jain and D. F. Jackson, Nucl. Phys. A **99**, 113 (1967).
[17] N. S. Chant and P. G. Roos, Phys. Rev. C **15**, 57 (1977).
[18] E. D. Cooper, S. Hama, and B. C. Clark, Phys. Rev. C **47**, 297 (1993).
[19] K. Minomo, K. Ogata, M. Kohno, Y. R. Shimizu, and M. Yahiro, J. Phys. G **37**, 085011 (2010).
[20] K. Amos, P. J. Dormans, H. V. von Geramb, S. Karataglidis, and J. Raynal, Adv. Nucl. Phys. **25**, 276 (2002).
[21] R. A. Arndt, J. S. Hyslop III, and L. D. Roper, Phys. Rev. D **35**, 128 (1987).
[22] B. A. Brown, A. Etchegoyen, and W. D. M. Rae, Computer code OXBASH, the Oxford University-Buenos Aires-MSU shell model code, *Michigan State University Cyclotron Laboratory Report No. 524*, 1985.
[23] T. Suzuki, R. Fujimoto, and T. Otsuka, Phys. Rev. C **67**, 044302 (2003).
[24] M. Leuschner et al., Phys. Rev. C **49**, 955 (1994).
[25] Z. Y. Sun et al., Phys. Rev. C **90**, 037601 (2014).
[26] C. Barbieri, Phys. Rev. Lett. **103**, 202502 (2009).
[27] Ø. Jensen, G. Hagen, M. Hjorth-Jensen, B. Alex Brown, and A. Gade, Phys. Rev. Lett. **107**, 032501 (2011).